Autonomous Dynamic Hitch-Hiking Control of a Bionic Robotic Remora

Pengfei Zhang, Zhengxing Wu, *Senior Member, IEEE*, Di Chen, Min Tan, and Junzhi Yu, *Fellow, IEEE*

***Abstract*—Remora suckerfish and its hitch-hiking behavior bring enormous inspiration into the engineering field. In this article, a bioinspired hitch-hiking behavior is accomplished automatically by a robotic remora, which creates possibilities for prolonging its endurance and multirobot cooperation. First, the definition of the hitch-hiking task and the mechatronic design of robotic remora are introduced. Then, aiming at the hitch-hiking task, the LED-marker-based underwater visual localization method and planar state synchronization controller are developed. The localization method includes a complete framework from LED detection to marker pose optimization, which considers the refraction correction to improve the localization precision in water. The synchronization controller is decomposed into the lateral and longitudinal subcontrollers to overcome the challenges caused by underactuated dynamic. Besides, a finite state machine is designed to model the state and action transition during the hitch-hiking task. Extensive experimental results demonstrate the effectiveness of the proposed method. The autonomous hitch-hiking task toward a moving host is successfully implemented by a robotic fish for the first time. Such results may offer valuable insights into the future autonomous operation of underwater robots.**

***Index Terms*—Autonomous control, bioinspired adhesion, robotic fish, underwater visual localization.**

Manuscript received 4 December 2022; revised 4 March 2023; accepted 28 March 2023. Date of publication 11 April 2023; date of current version 14 September 2023. This work was supported in part by the National Natural Science Foundation of China under Grant 62233001, Grant 62022090, Grant 62273351, and Grant T2121002, and in part by the Joint Fund of Ministry of Education for Equipment Pre-Research under Grant 8091B022134. *(Corresponding author: Junzhi Yu.)*

Pengfei Zhang, Zhengxing Wu, Di Chen, and Min Tan are with the State Key Laboratory of Management and Control for Complex Systems, Institute of Automation, Chinese Academy of Sciences, Beijing 100190, China, and also with the School of Artificial Intelligence, University of Chinese Academy of Sciences, Beijing 100049, China (e-mail: zhangpengfei2017@ia.ac.cn; zhengxing.wu@ia.ac.cn; chendi2018@ia.ac.cn; min.tan@ia.ac.cn).

Junzhi Yu is with the State Key Laboratory for Turbulence and Complex Systems, Department of Advanced Manufacturing and Robotics, College of Engineering, Peking University, Beijing 100871, China, and with the State Key Laboratory of Management and Control for Complex Systems, Institute of Automation, Chinese Academy of Sciences, Beijing 100190, China, and also with the College of Electronics and Information Engineering, Guangdong Ocean University, Zhanjiang 524088, China (e-mail: junzhi.yu@ia.ac.cn).

Color versions of one or more figures in this article are available at https://doi.org/10.1109/TIE.2023.3265053.

Digital Object Identifier 10.1109/TIE.2023.3265053

I. Introduction

THE fishlike robot has achieved vigorous development over the past two decades due to its high maneuverability, efficiency, and concealability [1], [2]. However, it still faces the issues of limited endurance and weak work capacity [3]. Remora suckerfish and its hitch-hiking behavior bring an inspiration for addressing these issues [4]. Remora can adhere to a large host and transport itself to the destination with the forces of the host. This hitch-hiking ability is meaningful for reducing energy consumption and improving the work capacity of robotic fish. Inspired by this, a robotic remora has been developed in our previous work [5]. The designed robotic remora possesses reliable attaching ability and agile mobility, which can adhere to a static host through remote control. Nevertheless, it lacks autonomous perception, localization, and control ability, which limits its further application.

For improving the autonomy of robotic remora, this article studies the autonomous dynamic hitch-hiking task and focuses on two critical technical problems therein. The first one is the precise underwater visual localization for a compact robotic fish. Visual localization is the common choice for short-distance operation, but the refraction effect in water significantly causes the precision degradation of the traditional visual algorithm. An accurate underwater visual localization algorithm considering the refraction correction is imperative. The second one is the autonomous hitch-hiking control method with respect to (w.r.t.) a moving host. The 3-D hitch-hiking task usually requires the cooperation of the depth controller, planar controller, and attaching controller, which involves a complex scheduling method. Besides, the limited perceived ability causes the partially observable host state, and the underactuated dynamic of the robotic fish brings a motion coupling problem. These characteristics pose a great challenge for the controller design.

Refraction is a limiting factor of the precision of underwater visual localization. Light is bent as passing across the interfaces of the water, camera waterproof housing, and air. It results in that the imaging process in water cannot be described accurately by the traditional pinhole camera model [6]. Besides, the refraction distortion is highly related to the shape of medium interface, and thus, many researchers have analyzed the refraction distortion caused by the commonly used planar and spherical waterproof housing [7], [8], [9]. These refraction models have been applied in a few works about underwater visual localization. Miao et al. applied a quasi single viewpoint cameral model to correct

the refraction distortion and design a monocular visual-inertial odometry [10]. Chavez et al. employed the PinAx refractive model [8] to calibrate monocular camera and estimate the pose of fiducial marker [11]. In our previous work, a geometrical refractive model was applied to eliminate the refraction error of a stereo marker-based visual localization method [12]. These aforementioned works focus on the refraction correction of the planar waterproof shell. Compared with the planar one, the spherical shell can reduce the bending degree of light, and thus, possesses the merits of smaller distortion and larger field of view (FoV) [13]. However, the underwater visual localization method considering spherical refraction is rare at present.

A critical subtask for realizing the hitch-hiking behavior is to make the position, heading, and velocity of the robotic remora consistent with those of the moving host. This task is named state synchronization control in this article. The similar control task can also be found in the spacecraft rendezvous and docking [14], the dynamic landing of the quadrotor [15], and the dynamic docking of underwater vehicle [16]. Nevertheless, the synchronization control of the robotic fish confronts with two challenges. The first one is the significant underactuated property. The robotic fish cannot achieve omnidirectional movement, whose thrust and steering torque are coupled. The second one is the limited sensor. The robotic fish can hardly acquire the absolute motion status of itself and the moving host, and thus, only the relative motion information can be utilized. Fortunately, the trajectory tracking [17], [18], [19] and formation keeping [20], [21] of the robotic fish provide references for our work. Suebsaiprom et al. decoupled fish dynamics by linearization, and designed the speed controller and orientation controller separately to realize the trajectory tracking [17]. Castaño et al. designed a modified heading error for stabilizing the heading and lateral error in trajectory tracking [18]. Li et al. applied the active disturbance rejection control and proportional navigation law to realize the target pose control [21]. However, these methods also require global information and cannot be directly applied in synchronization control.

This article aims to develop a feasible solution to realize the autonomous hitch-hiking behavior by a robotic remora. The main contributions are two folds. On the one hand, an LED-based underwater visual localization method with spherical refraction correction is proposed, which improves the traditional algorithm and reaches the millimeter scale accuracy in a short distance (< 40 cm). This precise underwater localization method lays a solid foundation for the following hitch-hiking control and other autonomous operations of robotic fish. On the other hand, an autonomous hitch-hiking control strategy based on finite-state machine (FSM) and a planar state synchronization control method (PSSC) are proposed, which accomplishes the autonomous hitch-hiking task toward a moving host by a robotic fish for the first time. Notably, the PSSC are decomposed into the lateral and longitudinal control problems, which is partly learned from the autonomous vehicle control. This control method overcomes the underactuated dynamics property of the robotic remora and only requires the relative motion information, which provides valuable insights for the future controller design of bionic underwater robots.

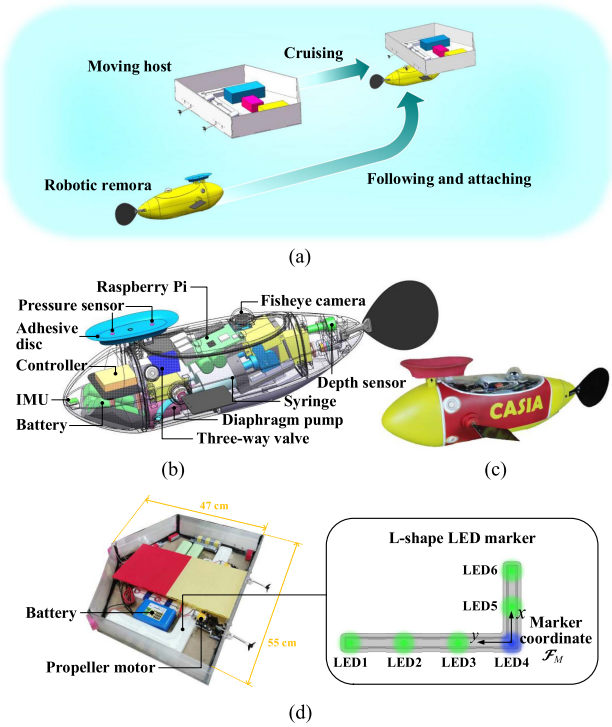

Fig. 1. Schematic of hitch-hiking task and mechatronic design. (a) Hitch-hiking task. (b) Conceptual design of robotic remora. (c) Robotic prototype. (d) Unmanned surface vehicle (Moving host) and LED marker.

II. Hitch-Hiking Task of the Robotic Remora

Hitch hiking is a natural behavior of remora, which offers insight into energy saving and the mother–son system in the robotic field. For transferring the hitch-hiking behavior to the engineered system, the definition of the hitch-hiking task and the mechatronic design of robotic remora are given in this section.

A. Hitch-Hiking Task Definition

The hitch-hiking task of the robotic remora is defined in Fig. 1(a). A robotic remora chases a moving host, attaches to the undersurface of the host, and travels by the host until arriving at the destination. In this article, the target host is an unmanned surface vehicle, which only performs the planar motion with a small steering speed. The undersurface of the host is a flat and transparent Acrylic plate. An L-shape LED marker is mounted on the bottom of the host, which provides the visual cues for the localization of the robotic remora. For achieving a broad perception range, a 220° fisheye camera is mounted on the dorsum of the robotic remora. Besides, the objective of the robotic remora is attaching to the center of the host and aligning its orientation with the host for reducing the fluid drag.

B. Mechatronic Design

The conceptual design of the robotic remora and prototype are shown in Fig. 1(b) and 1(c). The size ($L \times W \times H$) of robotic remora is 506 mm $\times$ 222 mm $\times$ 147 mm, and its weight is 2.86 kg. The major features differing from the common robotic

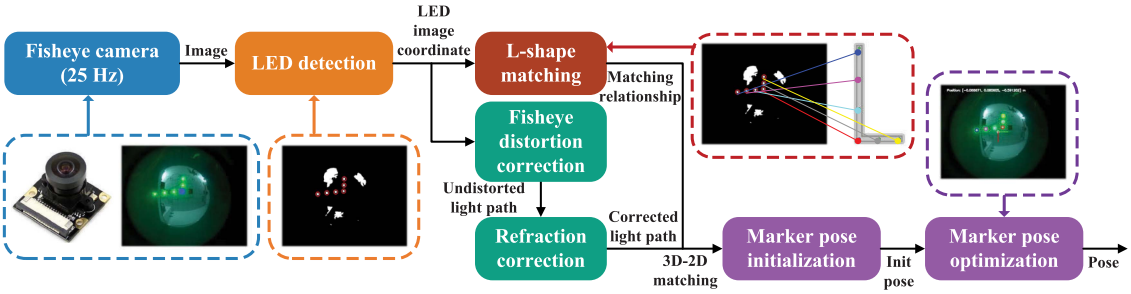

Fig. 2. Framework of the LED-based underwater visual localization algorithm.

fish are the adhesion system, the buoyancy adjusting system, the 360° joint of the pectoral fin, and the abundant sensors. The adhesion system is the most special improvement compared with the existing robotic fish, which is composed of an adhesive disk, a diaphragm pump, a three-way valve, and two pressure sensors. This system exhibits superior characteristics, including the low demand of preload, considerable pull-off ($\sim$250 N) and shear ($\sim$170 N) force, and perceptual ability. The buoyancy adjusting system adopts the syringe to store and release water, and further adjusts the robot depth actively. The omnidirectional pectoral fin joint can rotate by 360°, which can generate the forward, backward thrust, and steering torque. The onboard sensors include an inertial measurement unit (IMU), a depth sensor, two pressure sensors, and a fisheye camera. The pixel resolution of the fisheye camera is 640 × 480. The color mode is RGB and the field of view is 220°. Besides, a transparent spherical waterproof housing is applied to protect this camera. More details about the adhesion mechanism and actuator configuration can refer to our previous work [5].

An unmanned surface vehicle is adopted as the moving host. It is equipped with two propellers to generate the thrust. An L-shape LED marker is placed in the bottom as a visual feature so that the robotic remora can detect the host and acquire relative motion status. For ease of detection and matching, the LED marker consists of five green lamp beads and one blue lamp bead. Further, a marker coordinate $\mathcal{F}_M$ is defined, and the lamp bead positions w. r. t. $\mathcal{F}_M$ are already known.

III. LED-Based Underwater Visual Localization With Refraction Correction

In order to realize autonomous hitch-hiking tasks, autonomous perception and localization abilities are indispensable. In this article, an L-shape LED marker is designed as visual cue. The corresponding visual detection and localization methods are proposed. The algorithm framework is shown in Fig. 2. Notably, as the underwater refraction causes serious precision degradation, the refraction correction is a major consideration in this method. The algorithm consists of six modules, which are introduced carefully in the following.

A. LED Detection

The objective of this module is to detect all lamp beads in the captured image and distinguish the color. First, the RGB image is divided into three channels. The contour of the lamp beads in the R (red) channel is more clear, and thus, the R channel is applied to detect lamp beads. The R channel is processed through contrast enhancement, Gaussian blur, binarization, and contour detection. The contour candidates of the lamp beads are selected roughly. Note that the aforementioned image operations are supported by an open-source library called OpenCV. For obtaining precise detection results, the area and shape conditions are applied to filter the wrong candidates, which are as follows (α_* denotes threshold):

1) Area condition: $A_{\text{ct}} \geq \alpha_1$, where A_{ct} is contour area.
2) Circle condition: $\frac{A_{\text{cc}}}{A_{\text{ct}}} \leq \alpha_2$, where A_{cc} denotes the area of the circumscribed circle of the contour.
3) Median condition: $\frac{A_{\text{ct}}}{A_{\text{mc}}} \in [\alpha_3, \alpha_4]$, where A_{mc} is the median area of all contours.

Besides, the B (blue) and G (green) channels response actively to blue and green lamp beads, respectively. The difference between B and G channels is adopted to determine the color of the lamp bead. Notably, the exposure time is quite short in our experiment for avoiding the blurred image caused by the light scattering in water.

B. L-Shape Matching

The objective of this module is to build the corresponding relationship between the detected lamp beads in the image and the actual lamp beads in the physical world. Since the LED marker consists of five green lamps and one blue lamp (see Fig. 1), the blue lamp bead in the corner of the "L-shape" can be determined first. Then, according to the long and short edges of the "L-shape," the residual lamp beads can be divided into two groups. Finally, the lamp beads in each group can be distinguished by the distance from the blue one.

C. Fisheye Distortion Correction

The objective of this module is to reconstruct the light path according to the image coordinate of the lamp bead. The fisheye camera model is adopted here [22]. Denote the image coordinate of ith the lamp bead as $\mathbf{p}^i = [u, v]^T$, and the corresponding light vector in camera coordinate $\mathcal{F}_C$ can be written as follows:

$$\mathbf{p}^i = \begin{bmatrix} u \\ v \end{bmatrix} = \begin{bmatrix} c & d \\ e & 1 \end{bmatrix} \begin{bmatrix} u' \\ v' \end{bmatrix} + \begin{bmatrix} u_c \\ v_c \end{bmatrix} \tag{1}$$

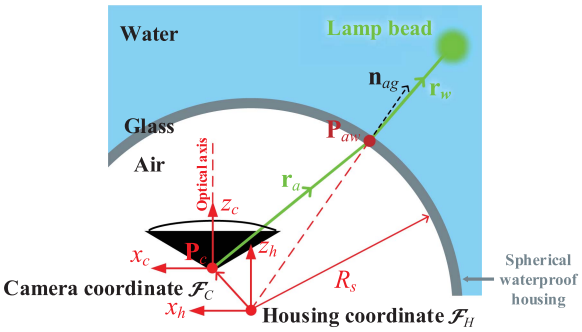

Fig. 3. Light path of a lamp bead in underwater visual localization.

$$ {}^{C}\mathbf{r}_a^i = \begin{bmatrix} x \\ y \\ z \end{bmatrix} = \alpha \begin{bmatrix} u' \\ v' \\ f(\rho) \end{bmatrix} \tag{2} $$

where

$$ f(\rho) = a_0 + a_1\rho + a_2\rho^2 + a_3\rho^3 + a_4\rho^4 + \cdots $$

$$ \alpha = 1/\sqrt{u'^2 + v'^2 + f^2(\rho)},\ \rho = \sqrt{u'^2 + v'^2} $$

where c, d, and e denote the affine transform coefficients. u_c and v_c are the coordinates of the optical center. $f(\rho)$ is the polynomial describing the projection property of the fisheye camera. The α is the normalization coefficient. ${}^{C}\mathbf{r}_a^i$ is the reconstructed light vector (see Fig. 3). The superscript C denotes that the vector is represented at camera coordinate $\mathcal{F}_C$.

D. Refraction Correction

As shown in Fig. 3, the fisheye camera is mounted behind a spherical glass housing. Owing to the refraction effect, the light path of the lamp bead can be divided as the air segment $\mathbf{r}_a$, glass segment, and water segment $\mathbf{r}_w$. The air segment $\mathbf{r}_a$ has been computed through the fisheye distortion correction. The glass segment is ignored as the thickness of glass housing is very small ($\sim$2 mm). Thus, the objective of this module is to compute the light segment in water according to the Snell's refraction law [23], [24]. The refraction correction of the ith lamp bead can be written as follows:

$$ \mathbf{P}_{aw}^i = \mathbf{P}_c + t_a^i \mathbf{r}_a^i \tag{3} $$

$$ \mathbf{n}_{aw}^i = \mathbf{P}_{aw}^i / \left|\left|\mathbf{P}_{aw}^i\right|\right| \tag{4} $$

$$ \mathbf{r}_w^i = \alpha_w \mathbf{r}_a^i + \beta_w^i \mathbf{n}_{aw}^i \tag{5} $$

where

$$ t_a^i = -\mathbf{P}_c \cdot \mathbf{r}_a^i + \sqrt{(\mathbf{P}_c \cdot \mathbf{r}_a^i)^2 - (\mathbf{P}_c \cdot \mathbf{P}_c - R_s^2)} $$

$$ \alpha_w = \frac{\mu_a}{\mu_w},\ \beta_w^i = -\alpha_w \mathbf{r}_a^i \cdot \mathbf{n}_{aw} + \sqrt{1 - \alpha_w^2 \left[1 - (\mathbf{r}_a^i \cdot \mathbf{n}_{ag})^2\right]} $$

where μ_a and μ_w are the refractive index of the air and water, respectively. R_s is the radius of the spherical housing. Besides, all vectors in above equation are represented at housing coordinate $\mathcal{F}_H$, but the superscript H is omitted for simplicity. There is no rotation between $\mathcal{F}_H$ and $\mathcal{F}_C$, and thus, ${}^{H}\mathbf{r}_a^i = {}^{C}\mathbf{r}_a^i$.

Based on the results of the refraction correction, the position of the lamp bead in 3-D space can be written as

$$ {}^{H}\mathbf{P}^i = {}^{H}\mathbf{P}_{aw}^i + \tau^i {}^{H}\mathbf{r}_w^i \tag{6} $$

where τ^i denotes the distance between the lamp position ${}^{H}\mathbf{P}^i$ and the point ${}^{H}\mathbf{P}_{aw}^i$. τ^i is an unknown parameter.

E. Marker Pose Initialization

Since the positions of lamp beads w. r. t. $\mathcal{F}_M$ and $\mathcal{F}_H$ are already known, the transformation between two coordinates can be calculated. The transformation can be written as follows:

$$ \mathbf{R}_M^H {}^{M}\mathbf{P}^i + {}^{H}\mathbf{p}_M = {}^{H}\mathbf{P}^i = {}^{H}\mathbf{P}_{aw}^i + \tau^i {}^{H}\mathbf{r}_w^i \approx \tau^i {}^{H}\mathbf{r}_w^i \tag{7} $$

where $\mathbf{R}_M^H \in \mathbb{R}^{3\times3}$ and ${}^{H}\mathbf{p}_M \in \mathbb{R}^3$ are the rotation matrix and translation vector between $\mathcal{F}_M$ and $\mathcal{F}_H$. Note that $||{}^{H}\mathbf{P}_{aw}^i||$ is equal to the sphere radius and τ^i is close to the marker–camera distance in general. Thus, ${}^{H}\mathbf{P}_{aw}^i$ can be omitted in initialization stage as the τ^i is far larger.

Based on the matching relationships of six lamp beads, 18 equations can be written in the same way of (7) and 18 unknown parameters ($\mathbf{R}_M^H$, ${}^{H}\mathbf{p}_M$, and $\tau^1 \sim \tau^6$) can be solved. The direct linear transformation (DLT) method can be used to solve this problem [25]. Thus, the initial marker pose is calculated.

F. Marker Pose Optimization

In the initialization stage, the ${}^{H}\mathbf{P}_{aw}^i$ is omitted, and thus, the marker pose is not precise enough. For acquiring the more precise localization results, a marker pose optimization problem is constructed. The light emitted from the lamp bead can be denoted as (6). The optimization problem is to minimize the lamp position estimated by the transformation matrix and the light path of lamp bead, which is as follows:

$$ \min_{\mathbf{R}_M^H, {}^{H}\mathbf{p}_M} \sum_{i}^{6} || \left(\mathbf{R}_M^H {}^{M}\mathbf{P}^i + {}^{H}\mathbf{p}_M - {}^{H}\mathbf{P}_{aw}^i\right) \times {}^{H}\mathbf{r}_w^i ||_2^2. \tag{8} $$

Finally, the Levenberg–Marquardt (LM) method can be applied to solve the optimization problem and acquire the optimized marker pose [25].

IV. Autonomous Dynamic Hitch-Hiking Control

Based on the localization results, an autonomous control strategy is required to realize the hitch-hiking task. As the obstacle and dynamic uncertainties are ignored in this article, a rule-based control scheme is feasible. In this section, a finite-state machine-based control strategy is designed and the critical state synchronization controller for the hitch-hiking task is proposed.

A. Finite-State Machine-Based Control Strategy

The finite-state machine is a popular model for describing the state transition and action switch of an agent. Fig. 4 depicts the procedure of the hitch-hiking task and the corresponding FSM. This FSM consists of five states ($S_0 \sim S_4$). In the cruise searching state, the robotic remora swims randomly and searches for the moving host. Once the moving host is detected by

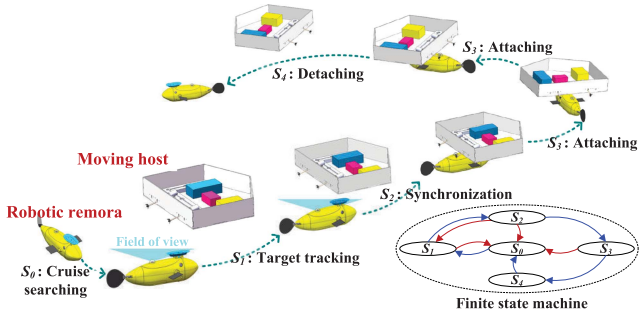

Fig. 4. Hitch-hiking control strategy and finite-state machine.

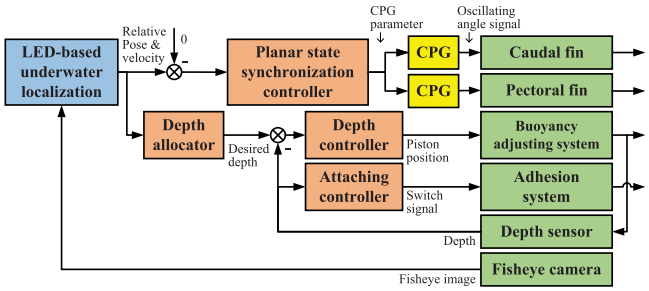

Fig. 5. Control framework in synchronization stage (S_2).

the fisheye camera, the robot enters the target tracking state. It follows and approaches the host until the relative distance decreases below a threshold. Then, the synchronization state is further activated. The robot finely adjusts its planar position, velocity, and depth to align with the moving host. When the state difference between the host and robot is lower than a threshold, the attaching switch is opened and the robot adheres to the host. In the attaching state, the robot travels by the moving host with tiny energy consumption. Finally, the robot detaches from the host when it arrives at the destination.

The state synchronization (S_2) is the most critical link in hitch-hiking procedure, whose controller framework is shown in Fig. 5. The depth sensor, fisheye camera, and LED-based localization method provide the feedback information in this framework. It consists of three subcontrollers, namely, the depth controller, attaching controller, and planar state synchronization controller. The depth controller drives the robot to reach the desired depth by adjusting buoyancy, where the desired depth is calculated automatically by a depth allocator. The attaching controller switches on and off the adhesion system according to the depth. The PSSC computes the parameter of the central pattern generator (CPG) for reducing the relative state error between the robot and host [5]. The output signals of the CPG are finally applied to control the rotation of the pectoral and caudal fins.

B. Planar State Synchronization Control (PSSC)

The objective of PSSC is to make it converge to zero that the planar relative state (position, heading, and velocity) between the robotic remora and moving host. Owing to the limit of driving

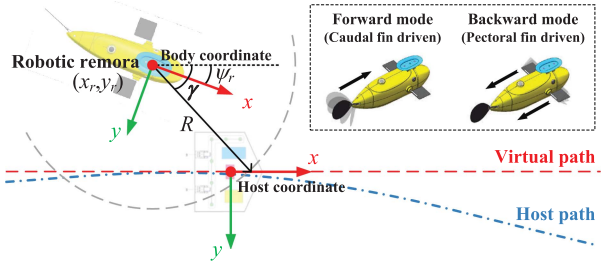

Fig. 6. Principle of the planar state synchronization controller.

mode, the robotic fish usually cannot move laterally and its kinematic is analogous to the car in some degree. Thus, inspired by the control method of autonomous car, the PSSC is decomposed into the lateral path following control (PFC) and longitudinal position-velocity control (PVC). Fig. 6 shows the core idea and symbol definition. In the PFC, a virtual path aligned with the x-axis of host coordinate is generated, and the robot follows the path to reduce the relative errors of lateral position and heading. In the PVC, the relative errors of longitudinal position and velocity are converged along the one-degree-of-freedom (one-DoF) virtual path. Besides, both the caudal and pectoral fins are applied in this control, which provide the forward and backward thrust, respectively.

1) Path Following Control Module: As shown in Fig. 6, the path following control is transformed into the heading control problem through the line-of-sight (LOS) guidance method [26]. The desired heading angle can be calculated as

$$\gamma = \arctan \frac{y_r}{\sqrt{R^2 - y_r}} \tag{9}$$

where y_r is the lateral position of robotic remora in host coordinate. R is the radius of virtual circle in LOS method.

The proportional-integral-derivative (PID) controller is further applied to adjust the robot heading to the desired one. The control law is as

$$u_\psi = k_p \psi_e + k_i \int \psi_e \mathrm{d}t + k_d \dot{\psi}_e \tag{10}$$

where k_p, k_i, and k_d are controller parameters. $\psi_e = \psi_r - \gamma$ is the heading error.

The designed PFC is obviously effective for a moving host in rectilinear motion. However, the convergence property w. r. t. a steering host should be further illustrated. Considering the host coordinate as base, the kinematic model of the relative pose between the host and robotic remora is [18]

$$\begin{cases} \dot{x}_r = y_r \omega_h + v_f \cos\psi_r - v_h \\ \dot{y}_r = -x_r \omega_h + v_f \sin\psi_r \\ \dot{\psi}_r = \omega_f - \omega_h \end{cases} \tag{11}$$

where x, y, ψ, v, and ω denote the position, heading, velocity, and angular velocity, respectively. The subscript h and f represent the host and robotic fish. The subscript r denotes relative quantity. Note that both the kinematic models of host and robot are assumed as $\dot{x} = v\cos\theta$, $\dot{y} = v\sin\theta$, and $\dot{\psi} = \omega$.

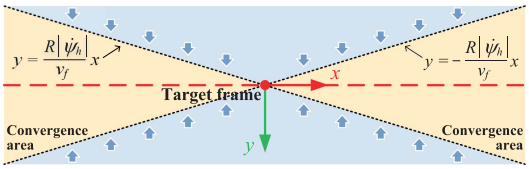

Fig. 7. Geometric interpretation of the convergence condition of path following control.

The objective of PFC is to make the lateral position y_r converge to zero. When the LOS method is adopted and the heading error ψ_e is assumed as zero, $\dot{y}_r$ can be written as

$$\dot{y}_r = -x_r\omega_h + v_f \sin\psi_r = -x_r\omega_h - \frac{v_f}{R}y_r \tag{12}$$

where

$$\psi_r = \gamma = \arctan\frac{y_r}{\sqrt{R^2 - y_r}},\ \sin\psi_r = -\frac{y_r}{R}.$$

Defining the Lyapunov function $V = \frac{1}{2}y_r^2$, its derivatives is $\dot{V} = y_r\dot{y}_r = -\frac{v_f}{R}y_r^2 - x_r y_r\dot{\psi}_h$. The sufficient condition of the convergence of y_r is $\dot{V} < 0$, namely, $-\frac{v_f}{R}y_r^2 < -|x_r||y_r||\dot{\psi}_h| \leq x_r y_r\dot{\psi}_h$. Thus, the sufficient condition can be written as

$$|y_r| > \frac{R|\dot{\psi}_h|}{v_f}|x_r|. \tag{13}$$

This convergence condition possesses definite geometric meanings, which is depicted in Fig. 7. The lateral position y_r will decrease below $\frac{R|\dot{\psi}_h|}{v_f}|x_r|$ when the robotic fish is in the blue area. It indicates that the robotic fish will enter the yellow area finally and the $\frac{R|\dot{\psi}_h|}{v_f}|x_r|$ is the upper bound of the $|y_r|$. In conclusion, the lateral error can be bounded as long as the robot velocity is not equal to 0 and the R and $\dot{\psi}_r$ are finite. Besides, the smaller R, smaller host angular velocity $\dot{\psi}$, and the larger velocity v_f can reduce the lateral error effectively.

2) Position-Velocity Control Module: Owing to the PFC module, the motion of the robotic remora can be regarded as a one-DoF movement along with the desired path. Thus, the objective of the PVC module is to further reduce the relative position and velocity error. The one-DoF dynamic models of host and the robot are as follows:

$$\text{Host: } \begin{cases} \dot{x}_h &= v_h \\ \dot{v}_h &= a_h \end{cases}, \text{Robot: } \begin{cases} \dot{x}_f &= v_f \\ \dot{v}_f &= \frac{1}{m}\left(u_f - k_v|v_f|v_f\right) \end{cases} \tag{14}$$

where a is acceleration. m and k_v are the robot mass and damping coefficient of water, respectively. u_f denotes thrust.

Then, the difference of position and velocity between the two agent can be written as a double integrator with the disturbance, which is as

$$\begin{cases} \dot{x}_1 = x_2 \\ \dot{x}_2 = u + d \end{cases} \tag{15}$$

where $x_1 = x_h - x_f$ and $x_2 = v_h - v_f$ are the relative position and velocity. $d = a_h + \frac{k_v}{m}|v_f|v_f + d_e$ denotes the disturbances from the host acceleration, fluid drag, and other external sources. The d is assumed to be bounded, namely, $|d| < \beta$. Besides, $u = \frac{1}{m}u_f$ is the new control input.

The sliding mode controller is applied to solve this control problem with the disturbance. The sliding surface can be defined as

$$s = x_2 + cx_1\ (c > 0). \tag{16}$$

To decrease chattering and accelerate the convergence, the exponential reaching law is adopted as

$$\dot{s} = -\epsilon\text{sign}(s) - ks\ (\epsilon > \beta,\ k > 0). \tag{17}$$

Thus, the final control law can be written as

$$u_f = -mu = -m\left[-cx_2 - ks - \epsilon\text{sign}(s)\right]. \tag{18}$$

3) Complete Control Law: In this task, a caudal fin and a pair of pectoral fins are applied to generate the forward and backward thrust, respectively. Since these fins are driven by the oscillating signal of CPG, the output of PFC and PVC should be further transformed into the CPG parameters. The adopted CPG model is the same as our previous work [5]. The amplitude, frequency, and bias of the CPG model are proportional to the torque and thrust. The outputs u_f and u_ψ are also proportional to the torque and thrust, respectively. Thus, a linear mapping can be applied to transform the u_f and u_ψ into the CPG parameters. In the forward mode, the amplitude and bias of the caudal fin are applied to control the velocity and heading. In the backward mode, the amplitude sum and difference between both pectoral fins are used to adjust the thrust and torque. Besides, the oscillating frequency of all fins is fixed for motion stability. The complete control law can be written as follows.

1) Caudal fin forward mode ($u_f > 0$):

$$\begin{cases} f_c = f_0 \\ a_c = \alpha_{ca}u_f \\ b_c = \alpha_{cb}u_\psi. \end{cases} \tag{19}$$

2) Pectoral fin backward mode ($u_f < 0$):

$$\begin{cases} f_{pl} = f_{pr} = f_1 \\ a_{pl} = -\alpha_{pa}u_f + \alpha_{pb}u_\psi \\ a_{pr} = -\alpha_{pa}u_f - \alpha_{pb}u_\psi \\ b_{pl} = b_{pr} = \pi \end{cases} \tag{20}$$

where f, a, and b are frequency, amplitude, and bias of CPG, respectively. The subscript c, pl, and pr denote caudal fin, left, and right pectoral fins, respectively. f_0, f_1, and α_* are positive constant.

C. Depth Allocator and Controller

The depth allocator and controller coordinate the robot depth with the relative position between the robot and the host. When the relative position and heading are close to zero, the depth of the robotic fish will decrease for adhesion. While the relative states are larger than certain thresholds, the depth will increase for acquiring a wider operation space. Thus, a depth allocator is

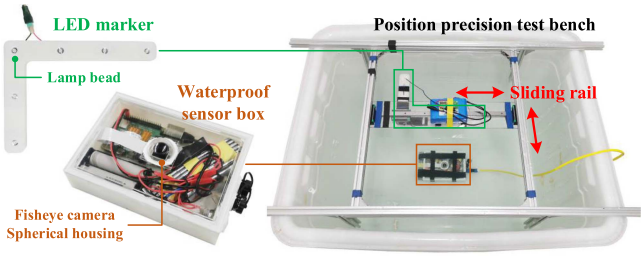

Fig. 8. Sensor module and test bench for underwater visual localization.

designed for determining the desired depth, which can be written as follows:

$$\dot{z}_d = \begin{cases} -v_z, & \text{if } (x_r, y_r, \psi_r) \in \mathcal{R} \\ 0, & \text{if } (x_r, y_r, \psi_r) \in \mathcal{B}\backslash\mathcal{R} \\ v_z, & \text{if } (x_r, y_r, \psi_r) \notin \mathcal{B} \end{cases} \tag{21}$$

$$z_d = \max\left(z_h - \bar{z}, z_d\right) \tag{22}$$

where z_d is desired depth. v_z is desired vertical velocity, and $v_z > 0$. $\mathcal{R} = \{(x, y, \psi) \big| |x| \le \Delta_x^r, |y| \le \Delta_y^r, |\psi| \le \Delta_\psi^r\}$ and $\mathcal{B} = \{(x, y, \psi) \big| |x| \le \Delta_x^b, |y| \le \Delta_y^b, |\psi| \le \Delta_\psi^b\}$ denote two sets of robot states, and $\mathcal{R} \subset \mathcal{B}$. z_h is the depth of host. $\bar{z}$ is the largest relative depth, which depends on the visual range of the robotic fish.

Besides, for avoiding disturbance from fish oscillation and water flow, a depth controller with a disturbance observer is adopted, whose actuator is the buoyancy adjusting system. The design detail can be found in our previous article [5].

V. Experimental Verification

A. Underwater Localization Precision Experiment

The localization experiments consist of two parts. The first part is validating the effectiveness of refraction correction, and the second part is evaluating the localization precision.

In the first test, a calibration checkerboard is placed in front of the fisheye camera. Then, the corner points of the black-and-white grid are detected and their 3-D positions are further reconstructed. The reconstructed results w. r. t. two camera-checkerboard (C-C) distances are shown in Fig. 9. Obviously, the reconstructed point with refraction correction is closer to the actual position compared with the results without correction. The average reconstructed errors for the C-C distance of 25 and 50 mm are 1.13 and 1.18 mm, respectively. This test reveals that spherical refraction correction is necessary for improving localization accuracy.

In the second test, a test bench and a sensor suite are developed to make the precision test credible (see Fig. 8). An LED marker is mounted at a two-DoF sliding rail and moves along a predefined "M-shape" path horizontally. The fisheye camera with a spherical housing (radius 13 mm, thickness 2 mm) is applied to measure the motion of the marker. The localization experiments are conducted at two vertical camera–marker (C-M) distances, whose results are shown in Fig. 10. The horizontal

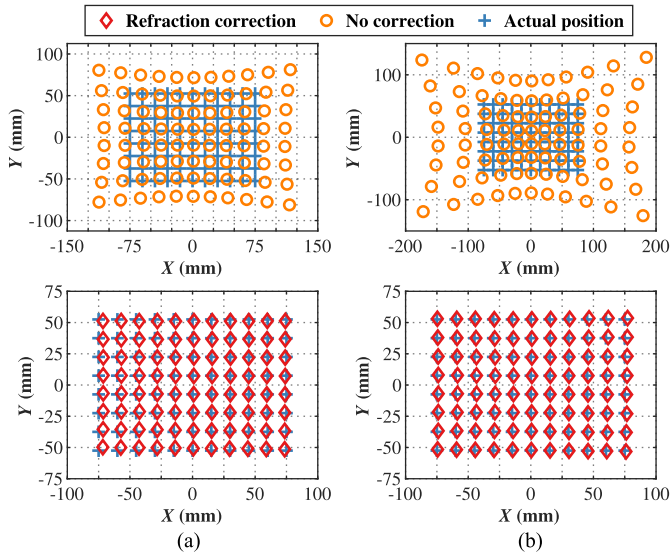

Fig. 9. Reconstructed checkerboard corners for various C-C distances. (a) C-C distance = 25 mm. (b) C-C distance = 50 mm.

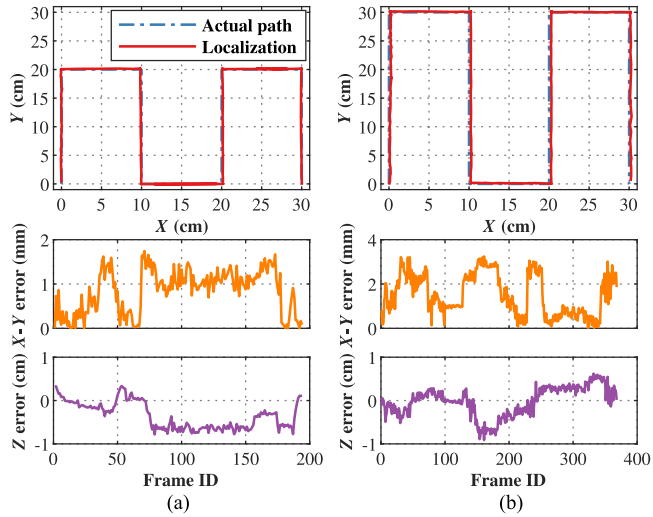

Fig. 10. Underwater localization results for various C-M distances. (a) C-M distance = 24 cm. (b) C-M distance = 44 cm.

errors between the actual path of the LED marker and the localization results are smaller than 2 and 4 mm w. r. t. the C-M distance of 24 and 44 cm, respectively. The vertical errors for two tests are smaller than 1 cm. This localization precision lays a solid foundation for the following hitch-hiking control.

B. Planar State Synchronization Control Experiment

The planar state synchronization experiments w. r. t. the hosts in rectilinear motion and circular motion are conducted in this subsection. A global vision system is adopted to provide the location of the robotic remora. Besides, a virtual host is generated based on a simple kinematic model, and its motion status is applied as control target. The results are given in Fig. 11. In the rectilinear test, the virtual host moves at 10 cm/s. The

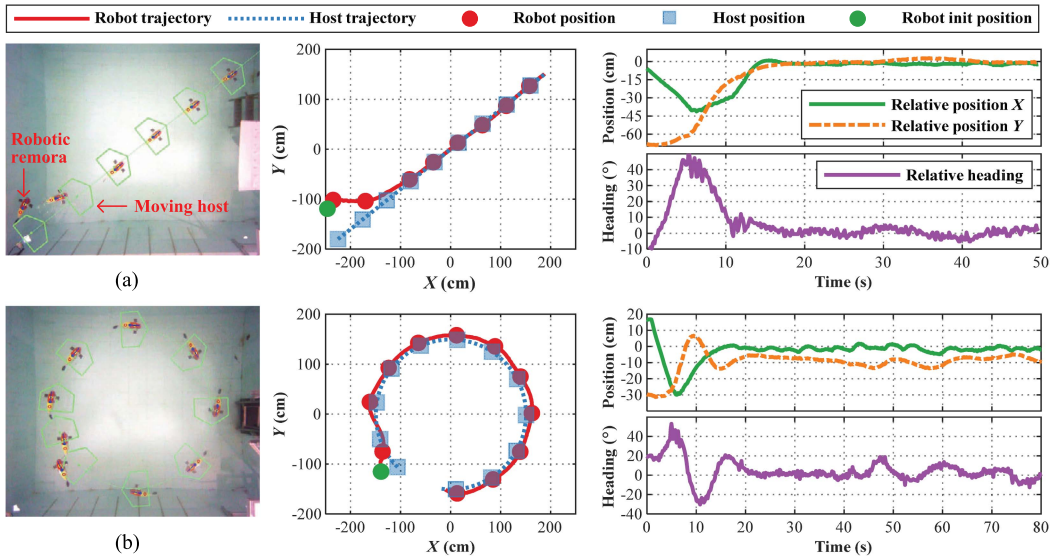

Fig. 11. Experimental snapshots and results of planar state synchronization control.

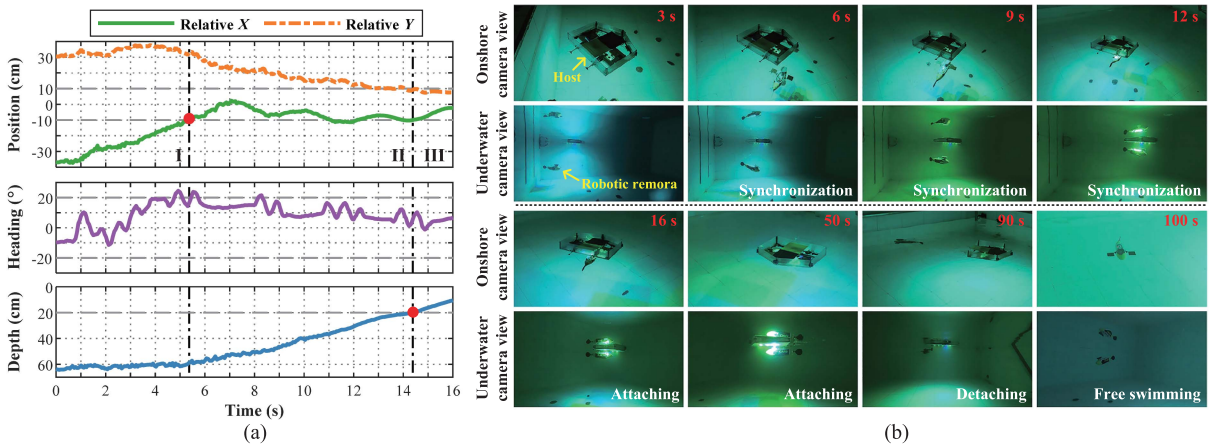

Fig. 12. Experimental snapshots and results of autonomous hitch-hiking control.

robotic remora catches up with the moving host after 18 s, and both the relative position and heading converge to zero. The error of position X, Y and heading after 18 s are 1.90 cm, 1.51 cm, and 2.17°, respectively. In the circular test, the virtual host moves at 10 cm/s and 3.82°/s. The relative position X and heading converge to zero after 20 s, whose errors are 1.59 cm and 4.00°. Besides, there exists a steady-state error of about 8.68 cm in the lateral position, which is consistent with the analysis in Section IV. These experiments validate that the proposed control method can realizes the precise state synchronization as the host moves straightly, and it can follow the steering host with a bounded error. In all, the proposed method can play an important role in the hitch-hiking task.

C. Autonomous Dynamic Hitch-Hiking Experiment

To validate the effectiveness of the proposed localization and control scheme, the autonomous dynamic hitch-hiking experiment is carried out. The experiment is conducted in an indoor pool (5 m×4 m), but all the localization and control data are calculated by the robotic remora. The moving host is an unmanned ship shown in Fig. 1, which moves at an average speed of 10 cm/s. The state curve and video snapshots of the experiment are shown in Fig. 12. Fig. 12(a) shows that the synchronization control consists of three stages. In stage I, the robotic remora always maintains it depth at 60 cm, and begins to adjust its horizontal position and heading. In stage II, as the error of X decreases below 10 cm, the robot depth is reduced to approach the host vertically. In stage III, when the depth is smaller than 20 cm as well as the position and heading is in the predefined range, the attaching system is opened to adhere to host. Fig. 12(b) shows the complete hitch-hiking process from the onshore and underwater view. The moving host runs on the surface of water, and the robotic remora starts behinds the host at the depth about 60 cm. The robot takes 16 s to keep pace with the host and adhere to it. Then, the host carries the robotic remora and keep sailing

to the destination. Finally, the robot detaches from the host at the destination.

D. Discussion

In the refraction correction experiment (see Fig. 9), the corner position error of the method without correction significantly increases with the distance between the camera and checkerboard. The reason is that the refraction effect changes the direction of light, and the difference between the original light and bent light widens with the travel distance. It indicates that refraction correction is essential for precise underwater visual localization. Furthermore, the localization precision test (see Fig. 10) validates that the accuracy of the proposed method is millimeter scale as the operation distance is lower than 44 cm. This precise localization method lays a solid foundation for the hitch-hiking control.

In the planar state synchronization control experiment (see Fig. 11), the x-axis position and heading can converge to zero, but there exists a steady-state error in the y-axis position for the host with circular motion. According to the analysis in Section IV, the control error in the y-axis position is bounded and related to the host angular velocity and self-speed. However, this control method still can effectively support the hitch-hiking task. More specifically, the robotic fish can decrease the position error and carry out precise adhesion as the host is moving straightly. While the host is steering, the robotic fish just keeps following and maintains a small lateral error. Actually, this is also the strategy adopted by the natural remora fish.

In the autonomous dynamic hitch-hiking experiment (see Fig. 12), the position control error and heading error are less than 10 cm and 10°. Although this control performance is fine for an autonomous underwater application, the error is a little larger than the results shown in Section V-B. The reason is that the actual hitch-hiking task is disturbed by the depth change and the localization error. However, the successful hitch-hiking experiment still validates the effectiveness of the FSM-based control scheme, the PSSC method, and the localization method, which may shed light on the autonomous operation of underwater robots.

VI. Conclusion

In this article, we had successfully implemented the autonomous hitch-hiking task toward a moving host, which was benefited from the proposed underwater visual localization method and planar state synchronization control method. The localization method corrected the spherical refraction distortion in water and achieved the precise pose estimation of an L-shape LED marker. The PSSC task was decomposed as two subproblems for overcoming the coupling property of fish dynamics. The path following and one-DoF position-velocity controller were further designed to achieve state synchronization. The effectiveness of the localization method and state synchronization controller was demonstrated by abundant experiments. Such results will not only effectively support the hitch-hiking task of the robotic remora, but also provide valuable insights into the autonomous application of other underwater robots.

The ongoing and future work will focus on enhancing robot intelligence in task execution and constructing the mother–son multirobot system.

References

[1] X. Li, Q. Ren, and J.-X. Xu, "Precise speed tracking control of a robotic fish via iterative learning control," *IEEE Trans. Ind. Electron.*, vol. 63, no. 4, pp. 2221–2228, Apr. 2016.

[2] J. Yu, C. Wang, and G. Xie, "Coordination of multiple robotic fish with applications to underwater robot competition," *IEEE Trans. Ind. Electron.*, vol. 63, no. 2, pp. 1280–1288, Feb. 2016.

[3] H. Dong, Z. Wu, J. Wang, D. Chen, M. Tan, and J. Yu, "Implementation of autonomous docking and charging for a supporting robotic fish," *IEEE Trans. Ind. Electron.*, vol. 70, no. 7, pp. 7023–7031, Jul. 2023.

[4] B. E. Flammang et al., "Remoras pick where they stick on blue whales," *J. Exp. Biol.*, vol. 223, no. 20, 2020, Art. no. jeb226654.

[5] P. Zhang, Z. Wu, Y. Meng, H. Dong, M. Tan, and J. Yu, "Development and control of a bioinspired robotic remora for hitch-hiking," *IEEE/ASME Trans. Mechatron.*, vol. 27, no. 5, pp. 2852–2862, Oct. 2022.

[6] M. Shortis, "Calibration techniques for accurate measurements by underwater camera systems," *Sensors*, vol. 15, no. 12, pp. 30810–30827, 2015.

[7] A. Jordt-Sedlazeck and R. Koch, "Refractive calibration of underwater cameras," in *Proc. Eur. Conf. Comput. Vis.*, Florence, Italy, Oct. 2012, pp. 846–859.

[8] T. Łuczyński, M. Pfingsthorn, and A. Birk, "The pinax-model for accurate and efficient refraction correction of underwater cameras in flat-pane housings," *Ocean Eng.*, vol. 133, no. 3, pp. 9–22, 2017.

[9] M. She, D. Nakath, Y. Song, and K. Köser, "Refractive geometry for underwater domes," *ISPRS J. Photogramm. Remote Sens.*, vol. 183, pp. 525–540, 2022.

[10] R. Miao, J. Qian, Y. Song, R. Ying, and P. Liu, "UniVIO: Unified direct and feature-based underwater stereo visual-inertial odometry," *IEEE Trans. Instrum. Meas.*, vol. 71, 2022, Art. no. 21563261.

[11] A. G. Chavez, C. A. Mueller, T. Doernbach, and A. Birk, "Underwater navigation using visual markers in the context of intervention missions," *Int. J. Adv. Robot. Syst.*, vol. 16, no. 2, pp. 1–14, 2019.

[12] P. Zhang, Z. Wu, J. Wang, S. Kong, M. Tan, and J. Yu, "An open-source, fiducial-based, underwater stereo visual-inertial localization method with refraction correction," in *Proc. IEEE Int. Conf. Intell. Robots Syst.*, Prague, Czech, Sep. 2021, pp. 4331–4336.

[13] C. Kunz and H. Singh, "Hemispherical refraction and camera calibration in underwater vision," in *Proc. OCEANS*, Quebec City, QC, Canada, Sep. 2008, pp. 1–7.

[14] L. Sun, W. Huo, and Z. Jiao, "Adaptive backstepping control of spacecraft rendezvous and proximity operations with input saturation and full-state constraint," *IEEE Trans. Ind. Electron.*, vol. 64, no. 1, pp. 480–492, Jan. 2017.

[15] P. Serra, R. Cunha, T. Hamel, D. Cabecinhas, and C. Silvestre, "Landing of a quadrotor on a moving target using dynamic image-based visual servo control," *IEEE Trans. Robot.*, vol. 32, no. 6, pp. 1524–1535, Dec. 2016.

[16] Z. Yan, D. Xu, T. Chen, J. Zhou, S. Wei, and Y. Wang, "Modeling, strategy and control of UUV for autonomous underwater docking recovery to moving platform," in *Proc. China Control Conf.*, Dalian, China, Jul. 2017, pp. 4807–4812.

[17] P. Suebsaiprom and C. Lin, "Maneuverability modeling and trajectory tracking for fish robot," *Control Eng. Pract.*, vol. 45, pp. 22–36, 2015.

[18] M. L. Castaño and X. Tan, "Backstepping control-based trajectory tracking for tail-actuated robotic fish," in *Proc. IEEE/ASME Int. Conf. Adv. Intell. Mechatron.*, Hong Kong, Jul. 2019, pp. 839–844.

[19] S. Dai, Z. Wu, J. Wang, M. Tan, and J. Yu, "Barrier-based adaptive line-of-sight 3-D path-following system for a multijoint robotic fish with sideslip compensation," *IEEE Trans. Cybern.*, early access, Mar. 22, 2022, doi: 10.1109/TCYB.2022.3155761.

[20] Z. Zhang et al., "Global vision-based formation control of soft robotic fish swarm," *Soft Robot.*, vol. 8, no. 3, pp. 310–318, 2021.

[21] L. Li et al., "Bottom-level motion control for robotic fish to swim in groups: Modeling and experiments," *Bioinspir. Biomim.*, vol. 14, no. 4, 2019, Art. no. 046001.

[22] D. Scaramuzza, A. Martinelli, and R. Siegwart, "A toolbox for easily calibrating omnidirectional cameras," in *Proc. IEEE Int. Conf. Intell. Rob. Syst.*, Beijing, China, Oct. 2006, pp. 5695–5701.

[23] A. Agrawal, S. Ramalingam, Y. Taguchi, and V. Chari, "A theory of multi-layer flat refractive geometry," in *Proc. IEEE Conf. Comput. Vis. Pattern Recognit.*, Providence, RI, USA, Jun. 2012, pp. 3346–3353.
[24] C. Qiu, Z. Wu, S. Kong, and J. Yu, "An underwater micro cable-driven pan-tilt binocular vision system with spherical refraction calibration," *IEEE Trans. Instrum. Meas.*, vol. 70, 2021, Art. no. 5010813.
[25] R. Hartley and A. Zisserman, *Multiple View Geometry in Computer Vision*. Cambridge, U.K.: Cambridge Univ. Press, 2003.
[26] J. Liu, Z. Wu, J. Yu, and M. Tan, "Sliding mode fuzzy control-based path-following control for a dolphin robot," *Sci. China Inf. Sci.*, vol. 61, no. 2, 2018, Art. no. 024201.

Pengfei Zhang received the B.E. degree in detection, guidance, and control techniques from the School of Aeronautics and Astronautics, Central South University, Changsha, China, in 2017, and the Ph.D. degree in control theory and control engineering from the Institute of Automation, Chinese Academy of Sciences, Beijing, China, in 2022.

His research interests include the motion planning and intelligent control of bioinspired robots.

Zhengxing Wu (Senior Member, IEEE) received the B.E. degree in logistics engineering from the School of Control Science and Engineering, Shandong University, Jinan, China, in 2008, and the Ph.D. degree in control theory and control engineering from the Institute of Automation, Chinese Academy of Sciences (IACAS), Beijing, China, in 2015.

He is currently a Professor with the State Key Laboratory of Management and Control for Complex Systems, IACAS. His research interests include fast maneuvers of bioinspired robotic fish and gliding motions of robotic dolphins.

Di Chen received the B.E. degree in automation from the Yanshan University, Qinhuangdao, China, in 2015, and the M.E. degree in control science and engineering from Tongji University, Shanghai, China, in 2018, and the Ph.D. degree in computer applied technology from the Institute of Automation, Chinese Academy of Sciences, Beijing, China, in 2022.

He is currently a Postdoctoral Research Fellow with the College of Engineering, Peking University, Beijing. His research interests include bioinspired robots and aquatic-aerial unmanned vehicles.

Min Tan received the B.Sc. degree in control science and engineering from Tsinghua University, Beijing, China, in 1986, and the Ph.D. degree in control science and engineering from the Institute of Automation, Chinese Academy of Sciences (IACAS), Beijing, in 1990.

He is currently a Professor with the State Key Laboratory of Management and Control for Complex Systems, IACAS. He has authored and co-authored more than 200 papers in journals, books, and conference proceedings. His research interests include robotics and intelligent control systems.

Junzhi Yu (Fellow, IEEE) received the B.E. degree in safety engineering and the M.E. degree in precision instruments and mechanology from the North University of China, Taiyuan, China, in 1998 and 2001, respectively, and the Ph.D. degree in control theory and control engineering from the Institute of Automation, Chinese Academy of Sciences, Beijing, China, in 2003.

From 2004 to 2006, he was a Postdoctoral Research Fellow with the Center for Systems and Control, Peking University, Beijing. He was an Associate Professor with the Institute of Automation, Chinese Academy of Sciences, in 2006, where he was a Full Professor in 2012. In 2018, he joined the College of Engineering, Peking University, as a Tenured Full Professor. His current research interests include intelligent robots, motion control, and intelligent mechatronic systems.